Open Ceramics 15 (2023) 100391

Contents lists available at ScienceDirect

Open Ceramics

journal homepage: www.sciencedirect.com/journal/open-ceramics

Effect of milling parameters on the morphology and sinterability of the yttrium oxide powders for transparent ceramics

Dariia G. Chernomorets [a,b,*], Andreana Piancastelli [a], Laura Esposito [a], Jan Hostaša [a]

[a] CNR ISSMC, Institute of Science, Technology and Sustainability for Ceramics, Via Granarolo 64, Faenza, 48018, Italy
[b] Institute for Single Crystals of NAS of Ukraine, 60 Nauky Ave., Kharkiv, 61072, Ukraine

ARTICLE INFO

Handling Editor: Dr Catherine Elissalde

Keywords:
Yttrium oxide
Transparent ceramics
Powder processing
Microstructure
Vacuum sintering

ABSTRACT

Yttrium oxide has multiple applications both as a transparent material with good optical, mechanical, and thermal properties, and for photonics when doped with rare earth ions. To achieve full transparency, a careful control of the process, from the selection of powders to the final densification by sintering, is required. In this context, the characteristics of the starting powders have a great impact on the final properties. In the present work, the effect of milling conditions of two commercial Y_2O_3 powders on the properties of ceramics obtained by cold isostatic pressing (CIP) and vacuum sintering was investigated. The milling rate varied between 80 and 300 rpm, and the milling time between 1 and 22 h. It was found that the optimal treatment conditions are 300 rpm for 65 min, which provided a homogeneous nano-sized Y_2O_3 powder. IR-transparent Y_2O_3 ceramics obtained by a vacuum sintering have a transmittance of 78.30% (1100 nm).

1. Introduction

The interest in polycrystalline transparent materials is constantly increasing due to the potential application in different areas, such as solid-state laser materials, windows, scintillators, etc. [1–4]. Compared to single crystals, polycrystalline materials have many advantages, including a variety of shapes, low cost of fabrication, and improved mechanical properties [5,6].

Yttrium oxide can be used in different applications because of its physical and chemical stability, high melting point (2430 °C), relatively high thermal conductivity, and transparency at a wide range of wavelengths (0.2–8 μm). Moreover, Y_2O_3 ceramics are characterized by a lower emissivity at high temperatures compared to sapphire, ALON and spinel [7,8]. However, due to the high melting point it is difficult to grow Y_2O_3 single crystals. Y_2O_3 transparent ceramics, on the other hand, may be produced by sintering at temperatures much below the melting point.

To ensure transparency, ceramics based on yttrium oxide must be fully dense and free of defects. The most common defects in transparent ceramics are pores [9,10]. The presence of pores in ceramics greatly affects their optical properties, since the pores are the centers of light scattering, which leads to a decrease in optical transmission values. To avoid the pore formation, the right processing conditions and raw materials have to be chosen.

There are several methods for the fabrication of high-density transparent ceramics: vacuum sintering, hot isostatic pressing (HIP), hot pressing (HP), microwave, spark plasma sintering, or combinations of the above (often vacuum sintering followed by HIP). The HP, HIP, and SPS methods have many advantages, but their use is limited by the high cost of the equipment and in the case of HP and SPS only components with simple shapes can be produced. Therefore, the possibility of obtaining transparent Y_2O_3 ceramics just by vacuum sintering, which is a relatively widespread and available technique, is of high interest [11–15]. To use vacuum sintering only in an effective way, it is beneficial to increase sintering activity and reduce consolidation temperatures, for example using very fine powders (submicron- to nanometric powders) with high excess surface energy. Also, it is worth considering that working with nanometric powders is quite challenging and therefore their comprehensive analysis is necessary. The powder characteristics, such as particle size, morphology or specific surface area, influence the sintering behavior and, as a consequence, the possibility and conditions required for the achievement of fully dense, transparent ceramics [1,16].

However, it should be noted that the effect of different starting powders on the processability of Y_2O_3 transparent ceramics has not been studied much in detail. This work is focused on the powder treatment of

* Corresponding author. CNR ISSMC, Via Granarolo 64, Faenza, 48018, Italy.
E-mail address: dariia.chernomorets@issmc.cnr.it (D.G. Chernomorets).

https://doi.org/10.1016/j.oceram.2023.100391
Received 3 April 2023; Received in revised form 30 May 2023; Accepted 14 June 2023
Available online 15 June 2023

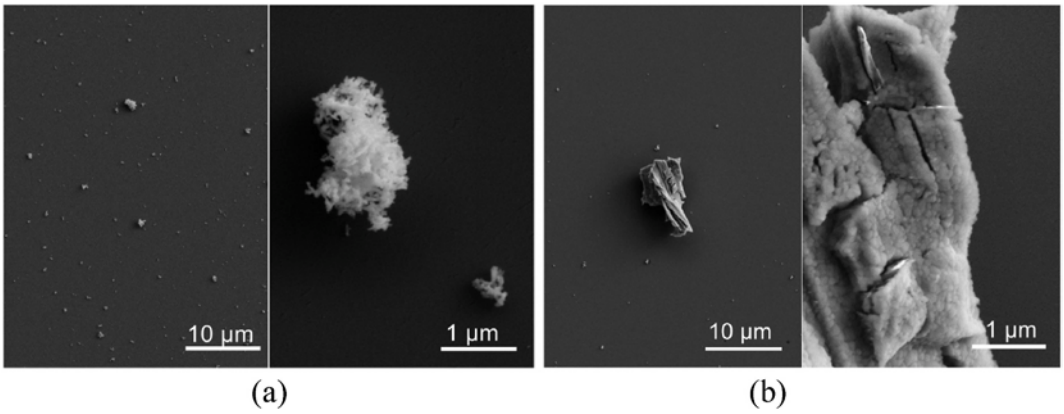

Fig. 1. FESEM of raw yttria powders: (a) Nippon, (b) Stanford.

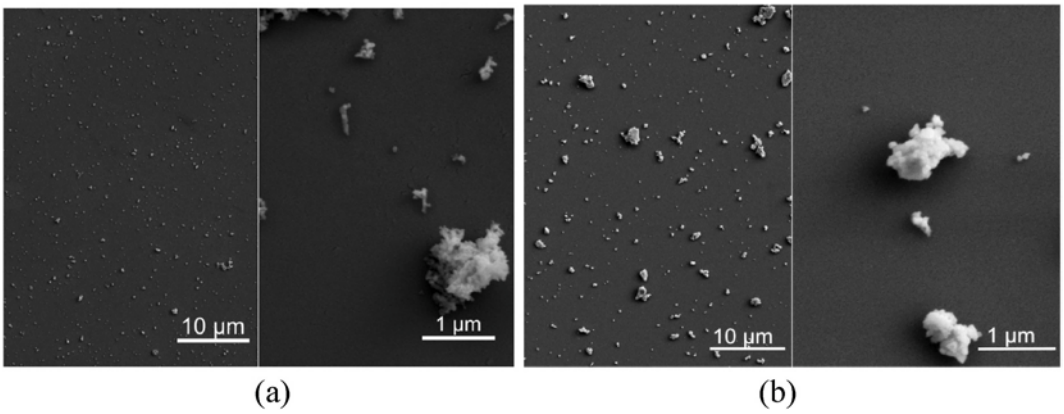

Fig. 2. FESEM of yttria powders after 22 h roller ball milling: (a) Nippon, NR; (b) Stanford, StR.

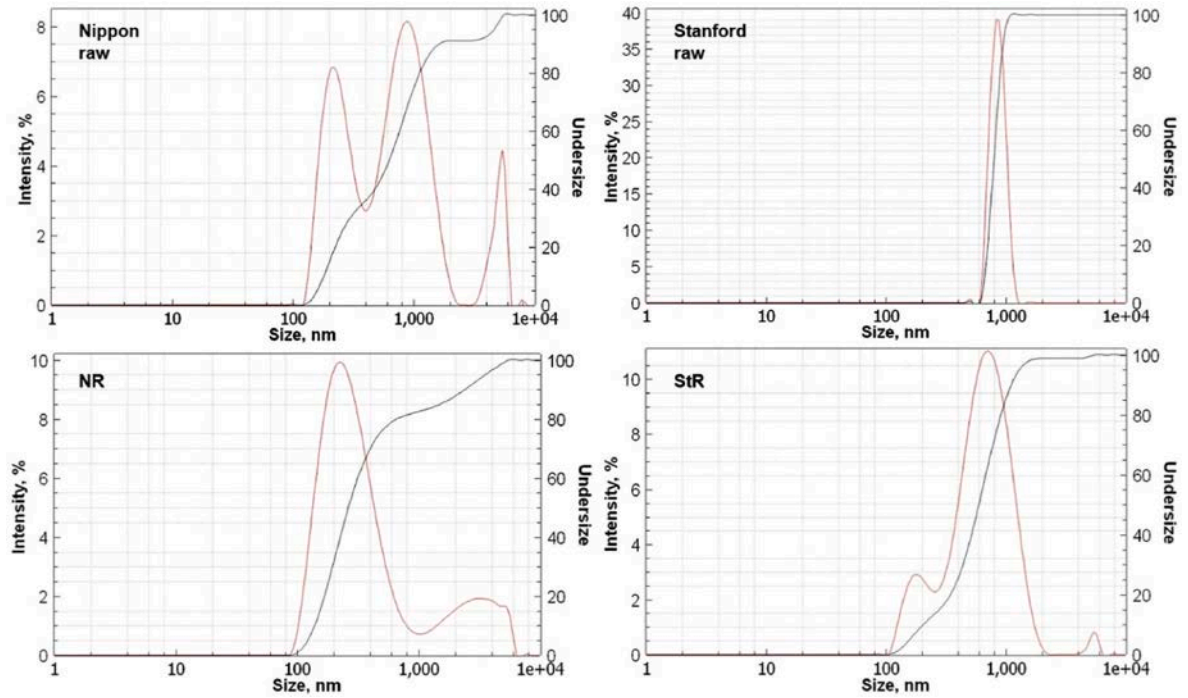

Fig. 3. DLS results Nippon and Stanford powders before (raw) and after roller milling (NR and StR, respectively).

Table 1
Parameters of ball milling; the NR and StR powders were milled by roller milling, all the other powders by planetary milling.

Powder	Rate, rpm	Time
NR (R – roller mixer)	80	22 h
1N	100	65 min
2N	200	65 min
3N	300	65 min
2.1N	200	10 h
3.1N	300	10 h
StR (R – roller mixer)	80	22 h
1St	100	65 min
2St	200	65 min
3St	300	65 min

Table 2
Powders characteristics. The Agglomeration degree has been calculated dividing agglomerate size (DLS) with the primary particle size (SEM).

Sample	Agglomerates size (DLS), nm	SSA (BET) of powders, m^2/g	Agglomeration degree
N-raw	546	23.11	8
NR	289	19.22	4
St-raw	1784	4.08	12
StR	527	6.24	4
1N	569	21.05	8
2N	489	19.64	7
3N	482	21.28	7
1St	981	–	7
2St	538	–	4
3St	458	7.17	3
2.1N	288	24.38	4
3.1N	247	25.66	3.5

Y_2O_3 and the production of transparent ceramics: two commercial powders with different morphology are selected for the study of the effect of milling parameters on the morphology and sinterability of the powders, eventually with the use of sintering aids.

To reduce the sintering temperature and improve the optical properties of Y_2O_3 ceramics, sintering additives are usually used, for example, Al_2O_3, Yb_2O_3, La_2O_3, ZrO_2, ThO_2, HfO_2, Nd_2O_3 or their combinations [17–23]. However, the use of Al_2O_3 or La_2O_3 easily leads to the formation of a second phase, whereas ThO_2 and HfO_2 have a high cost and are toxic. Therefore, in this work, we used ZrO_2 as sintering additive. With ZrO_2 the formation of secondary phases is generally prevented as long as the Zr^{4+} concentration is within the solubility limit. Indeed, changes in crystal lattice occur during the formation of a Y_2O_3: Zr^{4+} solid solution from the starting materials, and this activates diffusion processes that promote the densification without the formation of a secondary phase.

The aim of this study is to provide practical information related to the selected powders, and to make more general considerations, linking the microstructure and the type of defects in the sintered ceramics to the process parameters and powder characteristics, using only vacuum sintering to produce transparent ceramics.

2. Materials and methods

2.1. Ceramics fabrication

Highly pure commercial powders were used as starting materials: (a) Y_2O_3 (99.99%, Nippon Yttrium Co., Ltd., Japan) and (b) Y_2O_3 (99.99%, Stanford Advanced Materials, USA) further denoted as N- and St-powders, respectively. ZrO_2 (Tosoh TZ-0Y), was used as sintering additive (3 mol. %). PEG 400 (1 wt%) was used as dispersant. The powders were weighed according to stoichiometry and ball milled for 1–22 h with 2 mm zirconia balls in absolute ethanol as solvent. Rotation speed was tested in the range 80–300 rpm, using either roller ball mill with plastic jars (at 80 rpm) or a planetary ball mill with a zirconia jar (at speeds from 100 to 300 rpm). The powder:ball:ethanol ratio was 1:15:3 by weight. After milling, the slurries were dried in a furnace for 12 h at 80 °C. Green bodies were obtained by uniaxial pressing (d = 20 mm) at 55 MPa and cold isostatic pressing (CIP) at P = 250 MPa. Annealing in air was performed at 800 °C for 1 h. Afterwards, samples were sintered in vacuum at 1700–1735 °C with a soaking time of 24–32 h. All samples were mirror-polished after sintering and further analysed. The thickness of the samples after polishing ranged from 1.05 to 2.2 mm.

2.2. Characterization of the powders and sintered samples

The morphology of the starting and ball milled powders as well as the microstructure of sintered ceramics were analysed by scanning electron microscopy (SEM, Sigma, Zeiss) after ultrasonication treatment. The size of the primary particles and of the agglomerates has been determined from the SEM analysis of approximately 10 pictures. The Brunauer-Emmett-Teller (BET, Surfer 11510300, Thermo Scientific) specific surface area of the powders was measured by nitrogen adsorption apparatus. Dynamic light scattering method (DLS, Malvern Zetasizer Nano ZSP) was used to measure particle size. The density values of the green bodies and bulk densities of the sintered samples were determined by the geometrical and the Archimedes method, respectively. For SEM analysis ceramics samples were thermally etched at 1150 °C for 1 h. The transmittance spectra of the ceramics were obtained with UV-VIS-NIR spectrometer (Lambda 750, PerkinElmer).

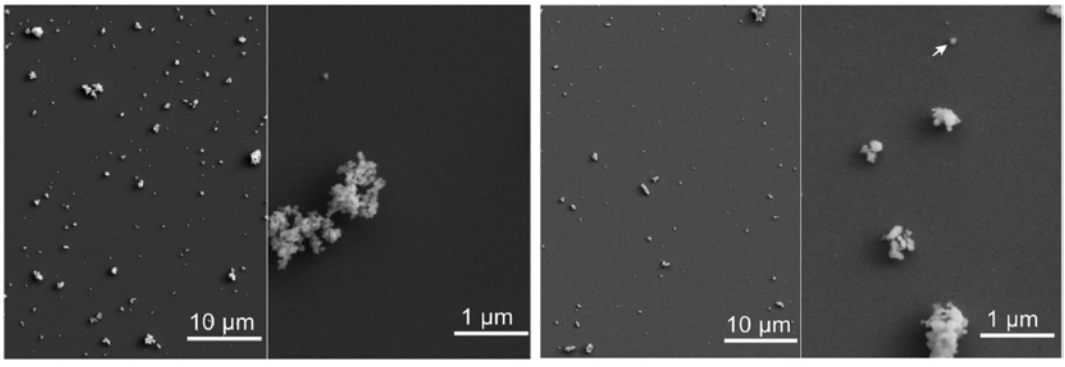

Fig. 4. SEM micrographs of Y_2O_3 powders milled at a milling rate of 300 rpm for 65 min: (a) 3N powder; (b) 3St powder.

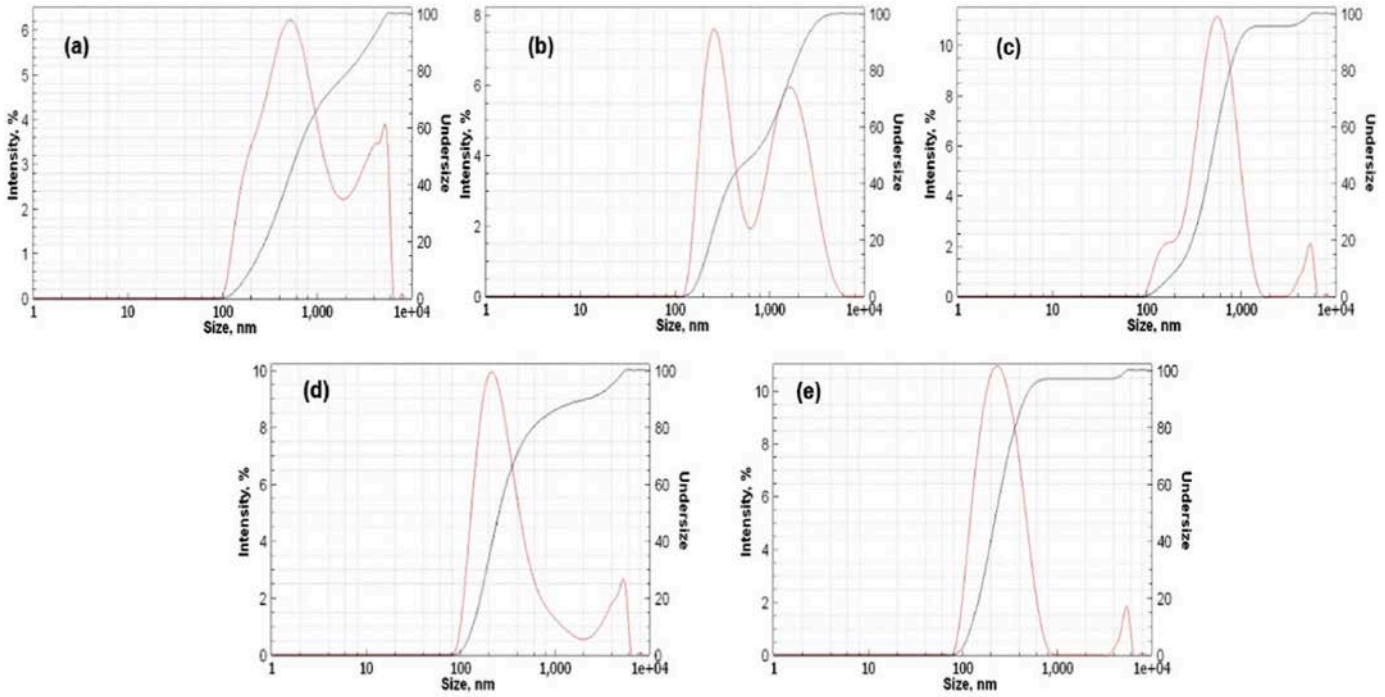

Fig. 5. DLS results for (a) 1N, (b) 2N, (c) 3N, (d) 2.1N, (e) 3.1N powders.

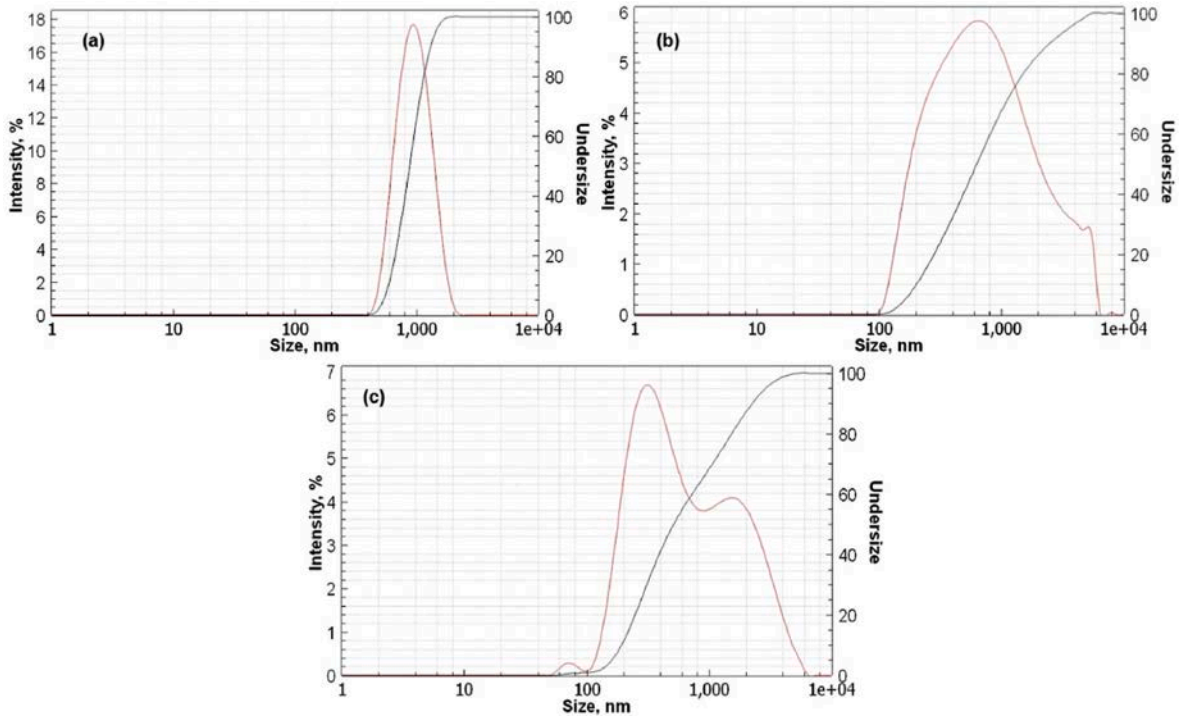

Fig. 6. DLS results for (a) 1St, (b) 2St, (c) 3St powders.

3. Results and discussions

3.1. Milling of powders

3.1.1. Raw Y_2O_3 powders

Fig. 1 shows SEM photographs of the two as-received Y_2O_3 commercial powders. Nippon powder (Fig. 1a) (further N-raw powder) has loosely connected agglomerates with an irregular shape which easily break during ball milling. According to the SEM results, this powder consists of round, slightly elongated primary particles. The average primary particle size of N-raw powder is approximately 70 nm. The Stanford powder (further St-raw powder) (Fig. 1b) is more agglomerated compared to N-raw Y_2O_3; the size of agglomerates is quite large, and their shape is irregular. These agglomerates consist of densely packed particles and have a lot of cracks whose presence seems to facilitate the milling process of St-raw powder. The individual particles seem to have

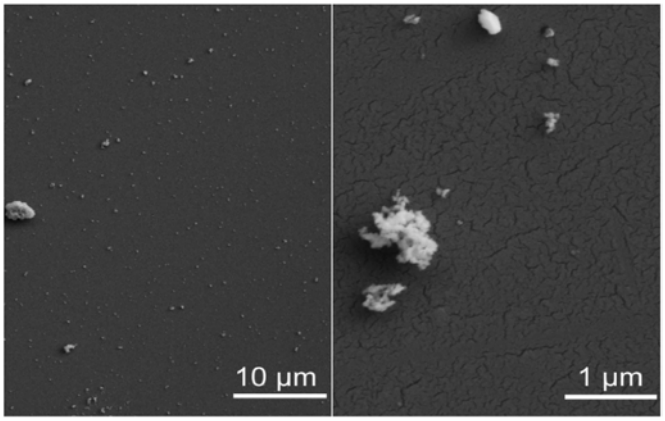

Fig. 7. SEM micrographs of 3.1N-powders milled at 300 rpm for 10 h.

plate-like shape. The average size of the primary particles for St-raw powder is about of 145 nm. Specific surface area (BET) of N-raw and St-raw powders is 23.11 m^2/g and 4.08 m^2/g, respectively (see Table 2).

According to the SEM, the agglomerates size of the N-raw Y_2O_3 powder is around 0.6 μm, which correlates quite well with the DLS results (average size is about 0.55 μm). Conversely, the agglomerates size of St-powder is in the range 1.0–10.0 μm, whereas by DLS it is smaller. This difference is probably due to the fact that large agglomerates sediment fast and therefore are not detected by the DLS analysis.

3.1.2. The 1st milling treatment (NR and StR powders)

Both yttrium oxide powders were milled in a roller mixer at 80 rpm for 22 h. SEM micrographs of these milled powders (further indicated as NR and StR) are shown in Fig. 2. The NR powder exhibits smaller aggregates compared to the StR. Both powders still exhibit some agglomeration, but the size of the agglomerates decreased as a result of the milling treatment. Agglomeration degree, which is number of primary particles in an agglomerate, decreased. It indicates that the milling process is effective. Conversely, the average size of the primary particles was not changed significantly after milling.

According to the DLS analysis, the particle size for N-raw and NR powders is in the range 0.3–4.0 μm (Fig. 3). Conversely, St-raw powder has a monomodal and narrow distribution of particle size around 1 μm whereas StR exhibits a wider particle size distribution.

Both for Nippon and for Stanford powder, there is a shift of the peaks to the area of smaller particle sizes after the milling treatment. This indicates that already the low-energy roller milling is efficient in reducing the particle size. In addition, NR powder does not exhibit the quasi-bimodal distribution of the N-raw, but a wide particle distribution in the range from 100 nm to 1 μm, plus a smaller number of particles with a larger size (Fig. 3). As for the Stanford powder, a wider particle size distribution is observed after milling, but with a significant decrease

Table 3
Relative density of green bodies after CIP.

Sample	1N	NR	2N	3N	2.1N	3.1N	StR	1St	2St	3St
ρ, % TD	47.48 ± 1.51	47.88 ± 0.83	48.12 ± 1.98	50.30 ± 1.28	49.45 ± 1.19	48.83 ± 1.32	54.11 ± 1.16	54.32 ± 2.62	55.86 ± 1.35	52.64 ± 6.18

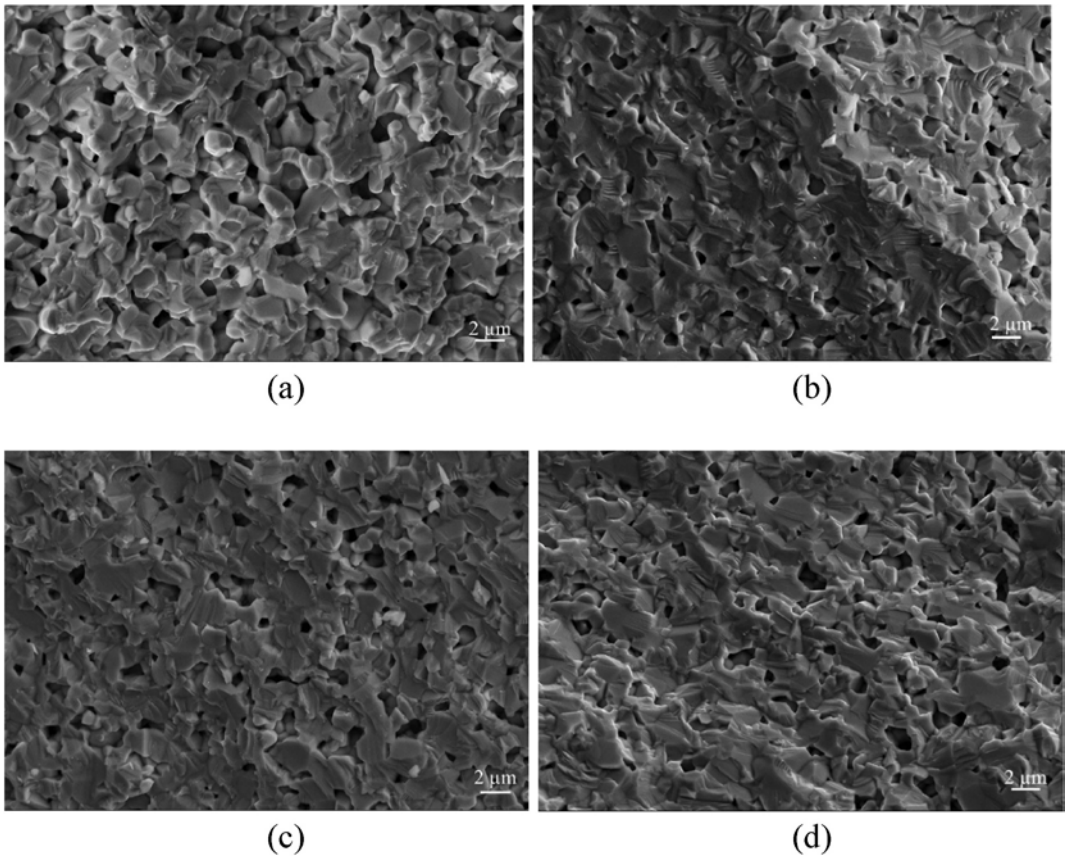

Fig. 8. Microstructure of fracture surface of sintered St-ceramics at 1700 °C for 24 h: (a) 1St, (b) StR, (c) 2St, (d) 3St.

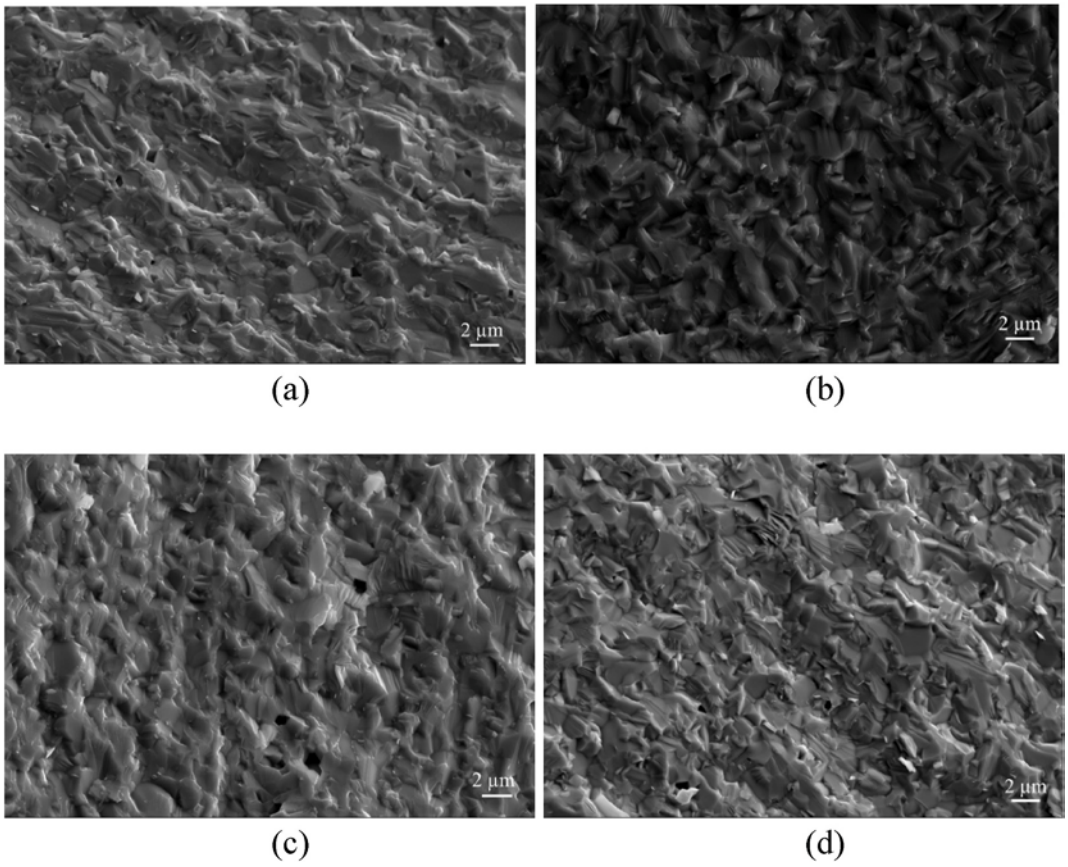

Fig. 9. SEM micrographs showing the microstructure of fracture surface of sintered N-ceramics at 1700 °C for 24 h: (a) 1N, (b) NR, (c) 2N, (d) 3N.

Table 4
Characteristics of vacuum sintered ceramics.

Vacuum sintering at 1700 °C for 24 h								
Sample	*1N*	*NR*	*2N*	*3N*	*1St*	*StR*	*2St*	*3St*
ρ, % TD	99.88 ± 0.2	99.66 ± 0.2	99.44 ± 0.1	99.83 ± 0.2	85.74 ± 0.3	93.66 ± 0.2	92.51 ± 0.3	93.65 ± 0.3
Grain size, μm	1–3	1–3	1–3	1–3	1–3	2–5	2–5	2–5
Vacuum sintering at 1735 °C for 32 h								
Sample	*1N*	*NR*	*2N*	*3N*	*2.1N*	*3.1N*		
ρ, % TD	100.0 ± 0.1	100.0 ± 0.3	100.0 ± 0.2	100.0 ± 0.1	100.0 ± 0.3	100.0 ± 0.2		
Grain size, μm	3.6 ± 0.2	4.2 ± 0.4	4.6 ± 0.3	3.8 ± 0.3	4.1 ± 0.3	4.1 ± 0.5		

in particle size, which is consistent with the results of SEM morphology analysis (Figs. 2–3).

3.1.3. The 2nd milling treatment (1N – 3N and 1St – 3St)

In a second set of experiments, N-raw and St-raw powders were milled by the planetary ball mill at milling rates in the range of 100–300 rpm for 65 min (Table 1). The N-powders exhibit a similar morphology after the various treatments, despite the different milling rate. The same applies to the St-powders. An example of the obtained morphologies is shown in Fig. 4. The N-powders have a more uniform morphology with smaller agglomerates compared to St-Y_2O_3. The small size of the N-powder can promote the interaction between the particles, leading to the formation of the agglomerates shown in the SEM pictures.

BET results for analysed powders are shown in Table 2. Increasing of milling rate leads to a slight decrease of the SSA, even with reference to the raw powder. This can be due to the aforementioned interactions among particles.

The DLS analyses reported in Fig. 5(a–c) and 6 show that for both Nippon and Stanford powders, with a milling time of 65 min, the increase of the milling rate from 100 to 300 rpm leads to a slight decrease of the agglomerate size (Table 2). In addition, for Nippon powder a more uniform particle distribution was observed with a milling rate of 300 rpm. This effect is observed due to the increased process energy and intensity of interaction between the particles, balls, and jar surfaces during milling. The probability of collisions that lead to milling increases at higher milling rate. As a result, smaller particles are formed [24].

The irregular hard agglomerates of the Stanford powder do not disappear after milling, even if their size decreases to about 460 nm. These data are in agreement with the SEM and BET results (Table 2). Following these results, Stanford powder does not seem to be suitable for obtaining fully dense transparent ceramic samples. Indeed, the presence of the hard agglomerates in the Stanford powder would easily lead to defects, in particular to residual porosity with an uneven distribution, that would prevent to obtain fully transparent components. In this regard, for the following milling tests, the Nippon powder was chosen.

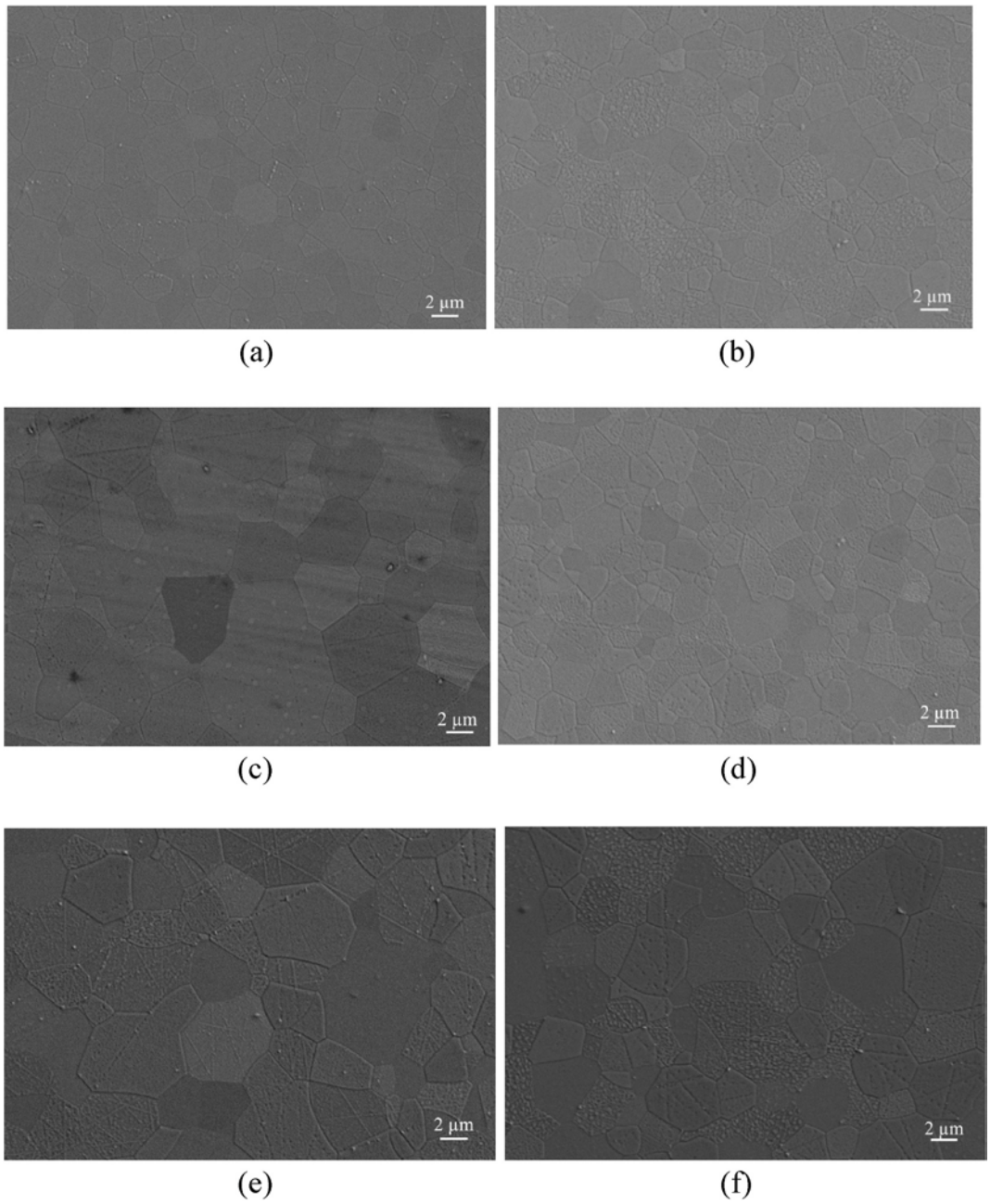

Fig. 10. SEM photographs of microstructure of thermal etched N-samples obtained by vacuum sintering at 1735 °C for 32 h: (a) 1N, (b) NR, (c) 2N, (d) 3N, (e) 2.1N, (f) 3.1N.

3.1.4. The 3rd milling treatment (2.1 N and 3.1 N)

The Nippon powder was milled at the rate in the range of 200–300 rpm for 10 h to investigate the effect of milling time. The obtained 2.1N and 3.1N powders have similar morphology, so SEM photographs are presented only for 3.1N-powder (Fig. 7). According to DLS results, increasing the milling time allows to obtain more uniform and finer powders (see Fig. 5 d-e). No decrease of primary particles size is observed, but the agglomeration degree decreased significantly compared to the raw powder (Table 2). The average particle size calculated from SEM analyses is around of 70 nm, and the SSA of 2.1N and 3.1N powders is higher compared to the SSA obtained with shorter milling time. According to these results, the increase of the milling time is particularly effective in the decrease of the agglomerates size, as shown by the morphology of the 3.1N-powder characterized by presence of some soft agglomerates. The decrease of agglomerates size with the extension of process duration was promoted by a more extensive collision among the particles, the milling balls and the jar walls.

3.2. Shaping

Green bodies were obtained by uniaxial pressing followed by CIP and their relative density in % of the theoretical density (further TD) is presented in Table 3. The relative density of N-samples is in the range from 47.5 to 50.3 TD % and in the case of St-samples it is higher (52.6–55.9 TD %).

The dependence of the relative density of these pressed compacts on the specific surface area of powders was investigated. In case of the Nippon powders, the relative density of the green bodies increases with the increase of the specific surface area for 1N–3N and then decreases for 2.1N–3.1N, as shown in Tables 2 and 3. This indicates that 3N powder

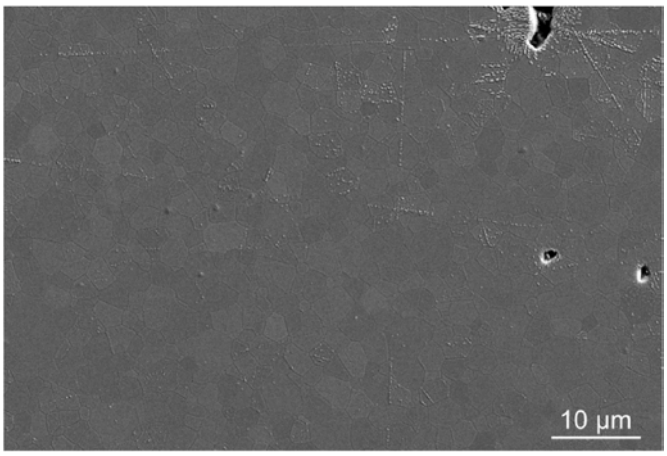

Fig. 11. SEM photograph of microstructure illustrated of residual porosity of 1N sample obtained by vacuum sintering at 1735 °C for 32 h; some large pores are visible on the right side of the image.

has optimal characteristics to achieve fully dense ceramics. A further increase in specific surface area (2.1N and 3.1N), even a slight one, led to lower green density. These latter powders are therefore less suitable for shaping by pressing than 1N–3N because their green microstructure may easily contain defects, which prevent the obtainment of pore-free final microstructure [1]. As for the agglomerates of Nippon Y_2O_3, these are loosely connected (Figs. 2a, 4a and 7), and do not affect the pressing operations. On the other hand, if the particles are nanometric with a high specific surface area as for Nippon powders, it may be necessary to change the pressing conditions (e.g., apply a lower pressure) in order to prevent cracking of the pressed bodies. The use of other shaping methods may also be contemplated.

Conversely, with the Stanford powder that is coarser, the green density is higher, but the presence of hard agglomerates (Figs. 2b and 4b) prevents the obtainment of a uniform microstructure that could lead to fully dense transparent ceramics after sintering. As it was noticed in the part 3.1.3, this type of powders is not suitable to obtain fully dense materials by pressing.

3.3. Vacuum sintered ceramics

The green bodies obtained from N- and St-powders by uniaxial pressing and CIP, were calcined in air at 800 °C for 1 h and sintered in vacuum at 1700 °C for 24 h. Only the N-ceramics were transparent, while all St-samples were opaque. The microstructure of all samples was analysed by SEM (Figs. 8–9).

Fig. 8 shows the microstructure of St-ceramics. These samples are highly porous. The pores are interconnected, and their size is comparable with the grain size (1–3 μm). As a result, these samples are opaque and their relative density is low (Table 4). The low density is caused by the high number of pores. The presence of hard agglomerates with irregular shape in the powders, which did not break during milling play also a role in preventing a dense packing of particle. Among the 4 Stanford powders, those exhibiting the higher densities (StR and 3St) have the lower agglomerates size and higher SSA. Still, since these ceramics are highly porous, they are opaque. As mentioned above, the pores in ceramics are centers of light scattering, which leads to deterioration of optical properties of material due to different refractive indexes of air and Y_2O_3 [10,25–28].

The microstructure of N-ceramics (Fig. 9) is more uniform compared to St-samples because the powder is finer and less agglomerated. All the fracture surfaces are transgranular, which indicates good mechanical properties. Some defects, in particular residual porosity, are present in all N-samples. Compared to St-samples, the Nippon ones exhibit much less pores, which in addition are isolated. The microstructure is more uniform with the less agglomerated powder (2.1N and 3.1N), since they can be pressed easier. Density of ceramics samples obtained at 1700 °C for 20 h is in the range 92.51–93.66% TD and 99.44–99.88% TD for St- and N-ceramics, respectively. These data are confirmed by the SEM results and optical properties of these samples, since the St-samples present the highest porosity and the lowest transmittance.

In addition to pressing, densification during vacuum sintering is important. The size, shape and curvature of powder particles have a significant influence on these processes, ultimately determining the sinterability of these powders. SEM and DLS analyses reveal that the N-powders have a smaller particle size, resulting in a higher excess surface energy compared to the St-powders. Thus, Nippon is characterized by a higher sintering ability which translates in denser ceramics samples. As a result of densification, transmittance increases. The same regularity is observed in the sintering of N-powders obtained under different milling conditions. The smaller the particles and the more uniform their size distribution, the more efficient the first stage of sintering. Thus, it can be concluded that increasing of milling rate of powders leads to a higher quality of samples due to formation of smaller particles.

Since the analysed samples are porous and pores are at the grains boundaries, it should be possible to remove these defects by increasing the sintering time and/or the temperature [20,29,30]. A second sintering cycle was therefore performed at a higher temperature (1735 °C) for a longer soaking time (32 h) on N-samples only, since they exhibited the more promising microstructure. As expected, increasing of sintering temperature leads to an increase of density and grain size (Table 4). The

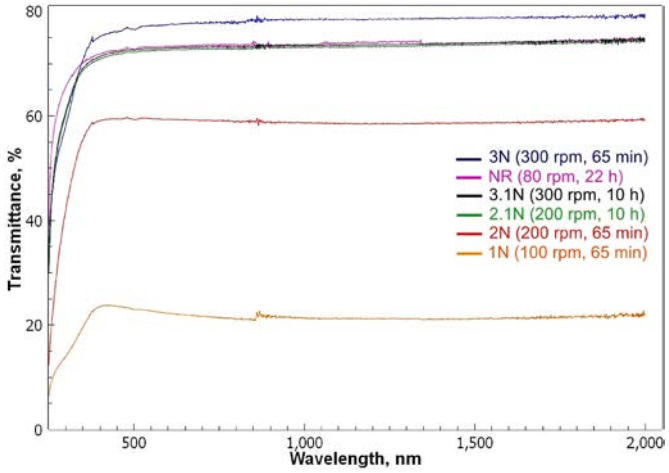

Fig. 13. In-line transmittance of Y_2O_3 ceramics obtained by vacuum sintering at 1735 °C for 32 h, normalized for 1 mm thickness. Captions to curves are arranged in order of decreasing transmittance.

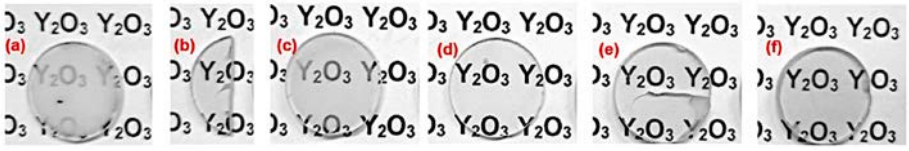

Fig. 12. N-ceramics obtained by vacuum sintering at 1735 °C for 32 h: (a) 1N, (b) NR, (c) 2N, (d) 3N, (e) 2.1N, (f) 3.1N.

obtained relative density is high and close to the theoretical values.

The SEM micrographs of thermally etched surfaces of the sintered samples are shown in Fig. 10.

Small spots formed on the surface of the ceramic in consequence of the thermal etching treatment and in some cases, the effect of the thermal etching is less effective due to scratches on the surface of the samples. In general, the samples have a quite uniform microstructure with no secondary phase. It should be noticed, however, that some residual porosity is still present despite the increased temperature and soaking time, probably as a consequence of the presence of some residual agglomerates [31]. Since the amount these residual pores is limited, it may be within the measurement error of the Archimedes' method, but it may influence the optical properties. Some pores with size of about 1 μm were observed in samples 1N and 2N along the grain boundaries (Fig. 11). According to the SEM results, other N-ceramics are characterized by an almost pore-free microstructure. As discussed in section 3.1, higher milling rate and time lead to a smaller particle size and higher specific surface area. Increasing the specific surface area improves the sinterability of powders and, as a result, it leads to an increase in the densification of samples [16].

3.4. In-line transmittance

Optical properties were analysed only for N-samples, since St-ceramics are opaque. The appearance of mirror-polished ceramics obtained from N-powders is shown in Figs. 12 and 13 shows the in-line optical transmittance spectra.

Optical transmittance spectra of the sintered samples obtained from NR, 2.1N and 3.1N powders are very similar, which indicates that the treatments performed on these powders have a similar effect for obtaining transparent samples. The highest transmittance has been achieved with the 3N-sample sintered at 1735 °C for 32 h from powder with a relatively uniform morphology, narrow particle size distribution and a specific surface area of 21.28 m^2/g.

To compare the optical properties of Y_2O_3 ceramics, the obtained data were normalized to a thickness of 1 mm. The theoretical transmittance of Y_2O_3 is 82.43% at 1100 nm, which was calculated using the formula $T_{max} = 2n/(1+n^2)$, and refractive index data for Y_2O_3 from Ref. [32]. For 3N sample (thickness 1.3 mm), the normalized in-line transmittance value reached 78.30% at 1100 nm, i.e. 95.0% of theoretical transmittance.

4. Conclusions

In this study the influence of the starting powders and routes of their treatment on the optical transparency of Y_2O_3 transparent ceramics were investigated, with the following conclusions.

1. The Nippon powder is better suited than the Stanford powder for obtaining high-density optically transparent ceramics due to its smaller primary particle size (around 70 nm), softer agglomerates, and higher specific surface area. In contrast, Stanford powder is still agglomerated after milling. In addition, the shape of agglomerates is irregular, which affects the shaping of green bodies by uniaxial pressing. A high-energy milling could improve the morphology of St-powder, but it can be a source of contamination.
2. The optimal ball milling parameters for obtaining powder with suitable characteristics were a milling speed of 300 rpm for 65 min. These results are supported by SEM, DLS and the specific surface area of 3N powder. The powder obtained under these conditions has a uniform morphology. Increasing the milling time to 10 h leads to powders with slightly higher values of specific surface area, but also to the formation of defects (pores) during pressing and, as a result, to a decrease of in-line transmittance.
3. A transparent high-density defect-free Y_2O_3:3 mol. % ZrO_2 ceramic was obtained from 3N powder by CIP and vacuum sintering at 1735 °C for 32 h. This ceramic exhibited a density close to the theoretical one, an average grain size of 3.8 ± 0.3 μm, and optical transmittance of 78.30% at 1100 nm (95.0% of the theoretical value).

Funding

This work was supportsupported by the JECS Trust. The visit of 27.06.2022 to 31.10.2022, contract No. 2021293.

Declaration of competing interest

The authors declare that they have no known competing financial interests or personal relationships that could have appeared to influence the work reported in this paper.

References

[1] A. Krell, H.W. Ma, Sintering transparent and other sub-μm alumina: the right powder, CFI Ceram. Forum Int. 80 (2003).
[2] A.C. Bravo, L. Longuet, D. Autissier, J.F. Baumard, P. Vissie, J.L. Longuet, Influence of the powder preparation on the sintering of Yb-doped Sc_2O_3 transparent ceramics, Opt. Mater. 31 (2009) 734–739, https://doi.org/10.1016/J.OPTMAT.2008.05.004.
[3] J. Kong, D.Y. Tang, J. Lu, K. Ueda, Spectral characteristics of a Yb-doped Y_2O_3 ceramic laser, Appl. Phys. B Laser Opt. 79 (2004) 449–455, https://doi.org/10.1007/s00340-004-1594-3.
[4] N.J. Cherepy, Z.M. Seeley, S.A. Payne, E.L. Swanberg, P.R. Beck, D.J. Schneberk, G. Stone, R. Perry, B. Wihl, S.E. Fisher, S.L. Hunter, P.A. Thelin, R.R. Thompson, N. M. Harvey, T. Stefanik, J. Kindem, Transparent ceramic scintillators for gamma spectroscopy and MeV imaging, in: Hard X-Ray, Gamma-Ray, Neutron Detect, Phys. XVII, SPIE, 2015, p. 95930P, https://doi.org/10.1117/12.2189156.
[5] L. Guo, Y. Shi, G. Chen, Y. Liu, X. Huang, Z. Dai, Z. Liu, F. Tian, D. Hreniak, J. Li, Fabrication of sub-micrometer sized Er:CaF_2 transparent ceramics for eye-safe lasers, Opt. Mater. 133 (2022), 113052, https://doi.org/10.1016/j.optmat.2022.113052.
[6] H. Eilers, Fabrication, optical transmittance, and hardness of IR-transparent ceramics made from nanophase yttria, J. Eur. Ceram. Soc. 27 (2007) 4711–4717, https://doi.org/10.1016/J.JEURCERAMSOC.2007.04.006.
[7] Y. Xu, X. Mao, J. Fan, X. Li, M. Feng, B. Jiang, F. Lei, L. Zhang, Fabrication of transparent yttria ceramics by alcoholic slip-casting, Ceram. Int. 43 (2017) 8839–8844, https://doi.org/10.1016/j.ceramint.2017.04.017.
[8] B. Ahmadi, S.R. Reza, M. Ahsanzadeh-Vadeqani, M. Barekat, Mechanical and optical properties of spark plasma sintered transparent Y_2O_3 ceramics, Ceram. Int. 42 (2016) 17081–17088, https://doi.org/10.1016/j.ceramint.2016.07.218.
[9] S. Hříbalová, W. Pabst, Modeling light scattering by spherical pores for calculating the transmittance of transparent ceramics – all you need to know, J. Eur. Ceram. Soc. 41 (2021) 2169–2192, https://doi.org/10.1016/J.JEURCERAMSOC.2020.11.046.
[10] R. Boulesteix, A. Maître, J.-F. Baumard, Y. Rabinovitch, F. Reynaud, Light scattering by pores in transparent Nd:YAG ceramics for lasers: correlations between microstructure and optical properties, Opt Express 18 (2010), 14992, https://doi.org/10.1364/oe.18.014992.
[11] Y.L. Aung, A. Ikesue, Importance of optical homogeneity for high-quality transparent ceramics, J. Eur. Ceram. Soc. 42 (2022) 6097–6103, https://doi.org/10.1016/j.jeurceramsoc.2022.05.067.
[12] Y. Han, J. Feng, J. Zhou, F. Li, X. Huang, L. Wang, G. Liu, J. Cheng, Heating parameter optimization and optical properties of Nd:YAG transparent ceramics prepared by microwave sintering, Ceram. Int. 46 (2020) 20847–20855, https://doi.org/10.1016/J.CERAMINT.2020.05.117.
[13] C. Liu, G. Zhou, J. Jiang, S. Hu, T. Zhang, S. Wang, Z. Xue, H. Lin, X. Qin, L. Gan, Fabrication and luminescence properties of highly transparent and submicrometer-grained Yb:Y_2O_3 ceramics by hot-pressing sintering, J. Alloys Compd. 898 (2022), https://doi.org/10.1016/j.jallcom.2021.163002.
[14] X. Chen, Y. Wu, Fabrication and optical properties of highly transparent MgO ceramics by spark plasma sintering, Scripta Mater. 162 (2019) 14–17, https://doi.org/10.1016/j.scriptamat.2018.10.022.
[15] I.O. Vorona, R.P. Yavetskiy, S.V. Parkhomenko, A.G. Doroshenko, O. S. Kryzhanovska, N.A. Safronova, A.D. Timoshenko, A.E. Balabanov, A. V. Tolmachev, V.N. Baumer, Effect of complex Si^{4+}+Mg^{2+} additive on sintering and properties of undoped YAG ceramics, J. Eur. Ceram. Soc. 42 (2022) 6104–6109, https://doi.org/10.1016/j.jeurceramsoc.2022.05.017.
[16] H.M. Oh, Y.J. Park, H.N. Kim, J.W. Ko, H.K. Lee, Effect of powder milling routes on the sinterability and optical properties of transparent Y_2O_3 ceramics, J. Eur. Ceram. Soc. 41 (2021) 775–780, https://doi.org/10.1016/j.jeurceramsoc.2020.08.006.
[17] K. Ning, J. Wang, D. Luo, J. Zhang, Z.L. Dong, L.B. Kong, D.Y. Tang, New double-sintering aid for fabrication of highly transparent ytterbium-doped yttria ceramics, J. Eur. Ceram. Soc. 36 (2016) 253–256, https://doi.org/10.1016/j.jeurceramsoc.2015.09.007.

[18] X. Hou, S. Zhou, Y. Li, W. Li, Effect of ZrO_2 on the sinterability and spectral properties of $(Yb_{0.05}Y_{0.95})_2O_3$ transparent ceramic, Opt. Mater. 32 (2010) 920–923, https://doi.org/10.1016/J.OPTMAT.2010.01.024.
[19] L.L. Zhu, Y.J. Park, L. Gan, S. Il Go, H.N. Kim, J.M. Kim, J.W. Ko, Effects of ZrO_2-La_2O_3 co-addition on the microstructural and optical properties of transparent Y_2O_3 ceramics, Ceram. Int. 43 (2017) 8525–8530, https://doi.org/10.1016/j.ceramint.2017.03.208.
[20] R.P. Yavetskiy, A.E. Balabanov, S.V. Parkhomenko, O.S. Kryzhanovska, A. G. Doroshenko, P.V. Mateychenko, A.V. Tolmachev, J. Li, N. Jiang, L. Gheorghe, M. Enculescu, Effect of starting materials and sintering temperature on microstructure and optical properties of Y_2O_3:Yb^{3+} 5 at% transparent ceramics, J. Adv. Ceram. 10 (2021) 49–61, https://doi.org/10.1007/s40145-020-0416-3.
[21] L. Jin, G. Zhou, S. Shimai, J. Zhang, S. Wang, ZrO_2-doped Y_2O_3 transparent ceramics via slip casting and vacuum sintering, J. Eur. Ceram. Soc. 30 (2010) 2139–2143, https://doi.org/10.1016/J.JEURCERAMSOC.2010.04.004.
[22] D. Yan, X. Xu, H. Lu, Y. Wang, P. Liu, J. Zhang, Fabrication and properties of Y_2O_3 transparent ceramic by sintering aid combinations, Ceram. Int. 42 (2016) 16640–16643, https://doi.org/10.1016/j.ceramint.2016.07.089.
[23] H.M. Oh, H.N. Kim, Y.J. Park, J.W. Ko, H.K. Lee, Influence of starting Y_2O_3 and Nd_2O_3 powders characteristics on optical properties of highly transparent Nd:Y_2O_3 ceramics, Opt. Mater. 121 (2021), https://doi.org/10.1016/j.optmat.2021.111562.
[24] L.B. Kong, W. Zhu, O.K. Tan, Preparation and characterization of $Pb(Zr_{0.52}Ti_{0.48})O_3$ ceramics from high-energy ball milling powders, Mater. Lett. 42 (2000) 232–239, https://doi.org/10.1016/S0167–577X(99)00190-1.
[25] R. Boulesteix, A. Maître, L. Chrétien, Y. Rabinovitch, C. Sallé, Microstructural evolution during vacuum sintering of yttrium aluminum garnet transparent ceramics: toward the origin of residual porosity affecting the transparency, J. Am. Ceram. Soc. 96 (2013) 1724–1731, https://doi.org/10.1111/jace.12315.
[26] A. Ikesue, K. Yoshida, Scattering in polycrystalline Nd:YAG lasers, J. Am. Ceram. Soc. 81 (1998) 2194–2196, https://doi.org/10.1111/j.1151-2916.1998.tb02607.x.
[27] W. Pabst, J. Hostaša, L. Esposito, Porosity and pore size dependence of the real in-line transmission of YAG and alumina ceramics, J. Eur. Ceram. Soc. 34 (2014) 2745–2756, https://doi.org/10.1016/j.jeurceramsoc.2013.12.053.
[28] A. Krell, T. Hutzler, J. Klimke, Transmission physics and consequences for materials selection, manufacturing, and applications, J. Eur. Ceram. Soc. 29 (2009) 207–221, https://doi.org/10.1016/j.jeurceramsoc.2008.03.025.
[29] F.F. Lange, Sinterability of agglomerated powders, Mater. Res. Soc. Symp. Proc. 24 (1984) 247–254, https://doi.org/10.1557/proc-24-247.
[30] P.R. Cantwell, M. Tang, S.J. Dillon, J. Luo, G.S. Rohrer, M.P. Harmer, Grain boundary complexions, Acta Mater. 62 (2014) 1–48, https://doi.org/10.1016/j.actamat.2013.07.037.
[31] J. Wang, J. Zhang, D. Luo, H. Yang, D. Tang, L.B. Kong, Densification and microstructural evolution of yttria transparent ceramics: the effect of ball milling conditions, J. Eur. Ceram. Soc. 35 (2015) 1011–1019, https://doi.org/10.1016/j.jeurceramsoc.2014.09.042.
[32] Y. Nigara, Measurement of the optical constants of yttrium oxide, Jpn. J. Appl. Phys. 7 (1968) 404, https://doi.org/10.1143/jjap.7.404.